FRET-based quantitative analysis of feedforward and feedback loops in EGFR signaling and the sensitivity to molecular targeting drugs.

Authors: Yoshihisa Fujita,[1] Naoki Komatsu,[2] Michiyuki Matsuda,[1,2] , Kazuhiro Aoki[3]

Affiliations:

[1] Department of Pathology and Biology of Diseases, Graduate School of Medicine, Kyoto University, Sakyo-ku, Kyoto 606-8501, Japan

[2] Laboratory of Bioimaging and Cell Signaling, Graduate School of Biostudies, Kyoto University, Sakyo-ku, Kyoto 606-8501, Japan

[3] Imaging Platform for Spatio-Temporal Information, Graduate School of Medicine, Kyoto University, Sakyo-ku, Kyoto 606-8501, Japan

Corresponding author: Kazuhiro Aoki, Imaging Platform for Spatio-Temporal Information, Graduate School of Medicine, Kyoto University, Sakyo-ku, Kyoto 606-8501, Japan; Tel.: 81-75-753-9450; Fax: 81-75-753-4698; E-mail: k-aoki@lif.kyoto-u.ac.jp

Running Title: Quantitative analysis of feedforward and feedback

Abbreviations

CFP, cyan fluorescent protein; ERK, extracellular signal-regulated kinase; MAPK, mitogen-activated protein kinase; FRET, Förster/fluorescence resonance energy transfer; MEK, mitogen-activated protein/extracellular signal-regulated kinase kinase; PI3K, phosphatidylinositol-3 kinase; RSK, ribosomal s6 kinase; TSC, Tuberous sclerosis protein;

Keywords: Akt/ EGFR/ ERK/ FRET/ simulation

Database: The mathematical model described here has been submitted to the JWS Online Cellular Systems Modelling Database and can be accessed free of charge at http://jjj.mib.ac.uk/webMathematica/UItester.jsp?modelName=fujita

Abstract

The Ras-ERK and PI3K-mTOR pathways are hyperactivated in various malignant tumors. Feedforward (FF) and feedback (FB) regulations between the Ras-ERK and the PI3K-mTOR pathways have been suggested to attenuate sensitivity to drugs targeting to these pathways and confer tumors resistance to therapies. However, because analyses of such regulations require measurements and perturbations with high temporal resolution, the quantitative roles played by FF and FB regulations in the intrinsic resistance to molecular targeting drugs remain still unclear. To address this issue, we quantified FF and FB regulations of the EGFR signaling pathway by FRET imaging. EGF-induced activation of EGFR, Ras, ERK, and S6K with or without inhibitors was measured by FRET imaging, and analyzed by semi-automatic image processing. Based on the imaging data set and kinetic parameters determined by our previous studies, we identified the roles played by a coherent FF regulation and two negative FB regulations, one of which was not recognized previously. The systems analyses revealed how these FF and FB regulations shape the temporal dynamics of ERK activity upon EGF stimulation. Furthermore, the simulation model predicts the response of molecular targeting drugs applied solely or in combination with each other to BRaf- or KRas-mutated cancer cell lines, indicating the validity of quantitative model integrating FF and FB regulations.

Introduction

The Ras-Raf-MEK-ERK MAP kinase cascade (hereinafter referred to as the Ras-ERK pathway) is an essential signal transduction pathway for proliferation and differentiation [1, 2], while the PI3K-Akt-mTORC1-S6K signaling pathway (hereinafter referred to as the PI3K-S6K pathway) plays pivotal roles in the process of apoptosis and survival [3]. Importantly, the deregulation of these signaling pathways through processes such as gene mutation and amplification induces tumorigenesis [4]. Therefore, molecules in these pathways are potential targets for cancer therapy. Several drugs targeting the Ras-ERK or the PI3K-S6K pathway, including MEK inhibitors, Raf inhibitors, and PI3K inhibitors, are

currently under clinical evaluations. However, the anti-cancer effects of these drugs varied significantly among cancer cells harboring different combinations of gene mutations, so that it is remarkably difficult to predict the drug response of individual cancers [5]. This problem is largely due to the complexity of the signaling networks controlling cancer cells [6], which makes it difficult to predict the effect of each molecular targeting drug on the total dynamics of the signaling pathways.

Complexity in signaling pathways arises from feedforward (FF) and feedback (FB) regulations and cross-talk among signaling pathways [7]. Previous studies had revealed the existence of various FB and cross-talk regulations in the Ras-ERK and PI3K-S6K pathways [8-12]. It has been suggested that FB regulations neutralized drug efficiency in tumor cells, a phenomenon known as intrinsic resistance [13-15]. Many of the previous studies have focused on the individual roles played by separate FB regulations. Cirit et al. contributed an elegant systematic quantification of negative FB mechanisms by data-driven modeling with biochemical data and global parameter fitting in PDGF-induced ERK activation [16]. They employed the expression of dominant negative mutants or pretreatment of chemical inhibitors to identify the negative FB in a simulation model. More recently, FF and FB regulations in the EGFR signaling network were quantified by modular response analysis [17]. However, a time-lapse measurement system combined with acute perturbations that were faster than the FB time scale has been direct method to distinguish whether a signaling component was merely required for a signaling pathway or whether it functioned as part of the FB loop [18].

In this study, we attempted to quantitatively evaluate FF and FB regulations in the Ras-ERK and PI3K-S6K pathways induced by epidermal growth factor (EGF). To this end, we employed biosensors based on the principle of Förster/fluorescence resonance energy transfer (FRET) [19] and chemical inhibitors to quickly perturb the activity of signaling molecules. Based on these data, we found one FF and two FB regulations that functioned in a coordinated fashion in the ERK activity dynamics induced by EGF stimulation. In addition, this model predicted the effect of molecular targeting drugs on the cell proliferation in cancer cells harboring mutation of the *KRas* or *BRaf* gene.

Results

Time-lapse FRET imaging in the Ras-ERK and the PI3K-S6K pathways

To quantitatively measure the temporal dynamics of the Ras-ERK and the PI3K-S6K pathways, we developed HeLa cell lines stably-expressing FRET biosensors for EGFR (PicchuEV-pm), Ras (RaichuEV-Ras), ERK (EKAREV-nuc), JNK (JNKAREV-nuc), PKA (AKAR3EV), or S6K (Eevee-S6K) [20] (Fig. 1, left). Three cell lines expressing FRET biosensors in the nucleus (ERK or JNK), cytoplasm (S6K or PKA), and plasma membrane (EGFR or Ras) were co-cultured in a 96-well or 4-well glass-bottom dish. In this way, we could monitor the activities of the three signaling molecules simultaneously, which improved the throughput of the data acquisition. To extract FF and FB regulations, we perturbed the signaling pathways acutely by adding chemical inhibitors. In this study, we applied 10 or 50 ng/ml EGF stimulation, which could maximally activate the downstream signaling pathways in HeLa cells [21]. The time-lapse images were semi-automatically processed to calculate FRET/CFP values representing the activities of molecules (Fig. 1, center). Finally, the quantified time-lapse data were applied to build the kinetic simulation model (Fig. 1, right). These results provided large-scale time-course data of the changes in EGFR, Ras, ERK, JNK, PKA and S6K activity upon EGF stimulation in combination with chemical inhibitors (Supplementary dataset 1). In this study, we do not utilize the data on JNK and PKA, because in the time-frame of the current study we could not find any substantial cross-talk between JNK or PKA and the Ras-ERK or PI3K-S6K pathways. These FRET biosensors appeared to linearly monitor endogenous activity of interest, except for EGFR and ERK biosensor, PicchuEV-pm and EKAREV-nuc, respectively. These two highly-sensitive FRET biosensors are saturated upon EGF stimulation (Fig. 2A and 2B) and could not monitor the decrease of phosphorylation of ERK and EGFR, which was detected previously by Western blotting [21]. To overcome this problem, we calibrated FRET/CFP values of EKAREV-nuc with the amount of phosphorylated ERK (Fig. 2C and 2D). By this way, the FRET/CFP ratio of EKAREV-nls were translated into the level of phospho-ERK and used to fit the simulation data with the experimental data (see below). We did not apply this approach to the other biosensors, which did not show saturation of the signals.

During the course of these analyses, we found the following two FB regulations and one coherent FF regulation in the Ras-ERK and the PI3K-S6K pathways: the negative FB regulation from ERK to EGFR [22], the positive FF regulation from Ras to Raf through PI3K and Rac1 [11], and the negative FB from RSK to Raf through TSC and Rheb [9, 10].

A negative feedback loop from ERK to EGFR

First, we noticed the FB regulation of ERK to EGFR (Fig. 3A). When EGF-stimulated cells

were treated with an MEK inhibitor, PD184352, EGFR activity was significantly increased as monitored by PicchuEV-pm (Fig. 3B, left, green line). In cells preincubated with PD184352 before EGF stimulation, the decrease in EGFR activity was slower than in untreated cells or cells preincubated with a PI3K inhibitor, LY-294002, or an EGFR inhibitor, PD153035 (Fig. 3B, right, green line). These results provided evidence of the negative FB regulation from ERK to EGFR and agreed with previous reports that EGFR are negatively regulated by the ERK-mediated phosphorylation of Thr-669 [22].

A coherent feedforward regulation from Ras to Raf through PI3K and Rac

Second, we observed the FF regulation of PI3K to ERK (Fig. 3C). When EGF-stimulated cells were treated with a PI3K inhibitor, PI-103, ERK was inhibited transiently in the early phase (<10 min), followed by partial recovery in the later phase (>20 min) (Fig. 3D, red line). It has been reported that PI3K activates Raf and thereby ERK1/2 in a Rac1- and PAK-dependent manner [11]. In agreement with this report, expression of a Rac1 dominant negative mutant markedly reduced the EGF-induced ERK activation (Fig. 3E). Furthermore, Ras dominant negative mutant almost completely abrogated EGF-induced S6K activation (Fig. 3F), showing that Ras activity was required for PI3K activation in EGF-stimulated HeLa cells [23].

A negative feedback loop from RSK to Raf through TSC and Rheb

Third, we found that RSK negatively regulated the ERK pathway by regulating the TSC-Rheb pathway (Fig. 3G). As reported previously [24], the RSK inhibitor BI-D1870 induced ERK activation, implicating RSK in the negative FB regulation of ERK (Fig. 3H). We considered the following scheme: RSK1 phosphorylates TSC2 at Ser-1798 to inhibit GAP activity of the TSC1/TSC2 complex, and thereby activates Rheb [9]. Activated Rheb in turn binds to and inhibits BRaf [10]. In further support of the negative FB model, pretreatment with the RSK inhibitor attenuated EGF-induced S6K activation (Fig. 3I, green line). The involvement of Rheb was examined by reducing the amount of Rheb by knockdown. Addition of a low-dose RSK inhibitor, wherein ERK could be activated only slightly in control cells, activated ERK markedly in the Rheb-knockdown cells (Fig. 3J). On the other hand, Torin1, an mTORC1/2 inhibitor, did not affect ERK activity, excluding mTOR from the negative FB (Fig. 3G-I).

A kinetic simulation model made up of the Ras-ERK and the PI3K-S6K pathways and FF

and FB regulations

To understand the coordinated effects of FF and FB regulations on the Ras-ERK and the PI3K-S6K pathways, we employed a systems biology approach. That is, we used a simulation model of the EGFR-Ras-ERK pathway with as many experimentally determined kinetic parameters as possible. More than 30 kinetic parameters in this signaling pathway have been determined in previous studies (Tables S1-S2) [8, 21]. In the present study, we introduced the signaling molecules belonging to the PI3K-S6K pathway and included the aforementioned FF and FB regulations (Fig. 4). Kinetic parameters in the PI3K-S6K pathway were estimated by fitting numerical simulation with experimental data (Tables S1-S2). Since EKAREV-nuc had high sensitivity, the amount of phosphorylated ERK calculated in simulation was converted into FRET/CFP values in EKAREV-nuc for parameter fitting (Fig. 5). The simulation overall reproduced the experimental data set, despite there were substantial discrepancies (see Discussion).

The model comprising the Ras-ERK and PI3K-ERK pathways could capture key dynamics of the experimental observations (Fig. 6A). For instance, MEK inhibition reactivated EGFR (Fig. 6B, left), and PI3K inhibition transiently inactivated ERK (Fig. 6B, right) as observed in the experiment (Fig. 3B and 3D, respectively). Further, the cross-talk between the Ras-ERK and PI3K pathways was evidenced by the effect of inhibition of Rac1 and Ras (Fig. 6C, D). The ERK activation and S6K inhibition by the RSK inhibition shown in Fig. 3H and 3I were also generally reproduced (Fig. 6E). Finally, the ERK activation by the RSK inhibitor in cells deficient in Rheb was also reproduced (Fig. 6F).

Computational and experimental demonstration of the roles played by cross-talk, FB regulation, and FF regulation.

The versatility of the simulation model could be demonstrated by predicting phenomena that might not be forecast intuitively. In the simulation model, MEK inhibition of EGF-stimulated cells caused a rapid but slight inhibition of S6K activity, followed by gradual increase (Fig. 7A, green line). Meanwhile, PI3K inhibition induced a marked inhibition of S6K, followed by slight recovery (Fig. 7A, red line). These adaptation-like behaviors suggested that the FF and FB regulations exerted coordinated effects on the Ras-ERK and PI3K-S6K pathways [25]. We examined the effects of the MEK and PI3K inhibitors experimentally (Fig. 7B). Expectedly, those adaptation-like behaviors predicted by the simulation were reproduced constantly. Furtheremore, we predicted that RSK inhibition would reduce EGF-induced Ras activation (Fig. 7C), because RSK inhibition cancels the

negative FB from RSK to Raf, and thereby upregulates the negative FB from ERK to Sos1. The prediction was validated experimentally (Fig. 7D): Preincubation with RSK inhibitor strongly suppressed EGF-induced Ras activation.

Next, we directly examined the contribution of the individual FF and FB regulations to the dynamics of ERK activation by abrogating each of them in silico (Fig. 7E, 7F). First, shut-off of RSK inhibition of TSC increased basal ERK activity, showing the central role of the negative FB regulation from RSK to Raf in controlling the ERK activity before EGF stimulation (Fig. 7E and 7F, left). Second, shut-off of PI3K-Rasc-Raf FF regulation strongly suppressed EGF-induced ERK activation, especially in the early phase (~ 10 min), indicating the large contribution of the PI3K-Rac-Raf pathway to the EGF-induced ERK activation (Fig. 7E and 7F, center). Third, shut-off of the negative FB regulation from ERK to EGFR/Sos1 caused sustained ERK activation after EGF stimulation (> 10 min) (Fig. 7E and 7F, right).

Prediction of the effect of molecular targeting drugs on cancer cell growth

We attempted to apply the simulation model to predict the effect of molecular targeting drugs on the growth of BRaf- or KRas-mutated cancer cell lines. As the source of experimental data, we employed pharmacological profiling data obtained from the Cancer Cell Line Encyclopedia (CCLE), which catalogues the dose-response data for 24 anticancer drugs across 479 cancer cell lines [5]. The dose-response data for MEK and BRaf inhibitors were extracted and averaged from BRaf-mutated cell lines and KRas-mutated cell lines (Fig. 8A, B). The BRaf-mutated cell lines were sensitive to a BRaf inhibitor, PLX-4720, and an MEK inhibitor, AZD6244; whereas the KRas-mutated cell lines were resistant to the BRaf inhibitor and less sensitive to the MEK inhibitor than the BRaf-mutated cell lines (Fig. 8A). This result was consistent with the analysis using different data set from other groups (Supplementary dataset 2) [26]. Further, we collected data on the effect of the PI3K inhibitor, PI-103, and the combination of the MEK inhibitor and PI3K inhibitor in a KRas-mutated cell line, HCT-116, and a BRaf-mutated cell line, HT-29 (Fig. 8B). Intriguingly, HCT-116 cells showed higher sensitivity to the PI3K inhibitor than did HT-29 cells (Fig. 8B, left). The combination of MEK and PI3K inhibitors efficiently inhibited the cell growth of both HCT-116 and HT-29 cells (Fig. 8B, right).

To simulate these pharmacological data, a KRas or BRaf mutation was first introduced into the simulation model (Fig. 4 and Table S1). The problem here was that the simulation model provided dose-response effects of molecular targeting drugs on the

activities of signaling molecules, but not on the cell survival and proliferation provided by the source data. Thus, to accommodate the experimental observations to the simulation model, we tried to identify a parameter that correlated with the cytotoxicity in experimental data. Eventually, we found that the sum of the fraction of phosphorylated ERK (pERK) and phosphorylated Akt (pAkt) correlated highly with the cell growth data (Fig. 8C). Thus, the sum of pERK and pAkt may serve as a useful index to predict the effects of molecular targeting drugs on the cell growth in KRas- and BRaf-mutated cells.

Lastly, we used the simulation model to investigate the involvement of the FF and FB regulations in the differential response between the BRaf-mutated cells and KRas-mutated cells. The results in the KRas-mutated cells demonstrated that both ERK and Akt were substantially phosphorylated in these cells (Fig. 9A). The partial resistance to MEK inhibitor was due to the further activation of Akt by MEK inhibition through the inhibition of negative FB from ERK to EGFR (Fig. 9A, right, blue line). Meanwhile, BRaf-mutated cells indeed showed the increase in pAkt in the presence of MEK inhibitor (Fig. 9B). However, the absolute value of the increase in pAkt was only 2% of total Akt (Fig. 9B, right, inset), and therefore these cells were almost exclusively dependent on ERK pathways. Taken together, these results provide quantitative insight into useful treatments in KRas- and BRaf-mutated cells by taking the FF and FB regulations into account (Fig. 9C). KRas-mutated cells should be treated with the combination of both MEK and PI3K inhibitors, whereas BRaf-mutated cells are expected to be sensitive to BRaf or MEK inhibitor alone.

Discussion

The roles played by FF and FB regulations in the Ras-ERK pathway have been studied by several research groups using different approaches. Santos et al. applied modular response analysis (MRA) to unveil the role of the Ras-ERK pathway in the neuronal differentiation of PC12 cells. They found that, upon EGF stimulation, the network exhibits negative feedback only, whereas upon NGF stimulation a positive feedback also appears and induces neuronal differentiation by bi-stable Erk activation [27]. Klinger et al. also adopted MRA in order to predict potent combinatorial treatments by inhibitors targeting the Ras-ERK and the PI3K-AKT pathways [17]. The MRA approach can handle a huge number of readouts and perturbations by high-throughput methods, which the ODE-based approach cannot. In

comparison to the ODE-based model used in the present study, Klinger's model includes negative FB regulation from ERK to EGFR and ERK to Raf, but lacks FF regulation from PI3K to Raf and negative FB regulation from RSK to Raf. The MRA approach draws the network structure primarily based on previous studies; therefore, the MRA-based model infers the contribution of each module, but cannot discover regulations that were not known or predicted previously. Furthermore, MRA relies on linear approximation under a system in the steady state, rendering it difficult to identify regulations that involve non-linear systems, such as complete adaptation, by this system.

On the other hand, the ODE-based approach is simple but heuristic. In fact, we were able to discover previously-unknown pathways, such as FB regulation from RSK to Raf, using this method. Cirit et al. also adopted the ODE-based approach, and were able to infer that negative regulation of MEK kinase plays a dominant role in the self-regulation of ERK activity in mouse fibroblasts [16]. Cirit's ODE-based approach is similar to our approach, i.e., data-driven modeling. In comparison to Cirit's model, our ODE model lacks negative FB regulation from ERK to Raf (Fig. 7F). Because FB from ERK to Raf complements FB from ERK to Sos1, in Cirit's model the FB regulation from ERK to Sos1 contributes to the suppression of ERK activity significantly less than in our model. The reason for this difference will only be clarified by experimentally accounting for all the actual parameters affecting these two FBs. Thus, we concluded that time-lapse data of many readouts with high temporal resolution and acute perturbations are essential to understand the effect of FF and FB regulation as an integral system of signaling pathway.

Multiple mechanisms of resistance to MEK inhibitors, such as acquired and intrinsic resistance, have been proposed [28-31]. The present study examined the role of the quantitative simulation model in the prediction of intrinsic resistance to molecular targeting drugs in cancer cells. Our data are consistent with the previous studies: BRaf-mutated cells showed higher sensitivity to an MEK inhibitor than KRas-mutated cells [32] (Fig. 8A), an MEK inhibitor caused PI3K activation through the release of negative FB from ERK [12] (Fig. 9A and 9B), and the combination of an MEK inhibitor with a PI3K inhibitor was a rational treatment for KRas mutated cells [33] (Fig. 8B and 8C). In the present work, we further proposed a mechanistic explanation for the difference in MEK inhibitor sensitivity between KRas- and BRaf-mutated cells; i.e., the strength of PI3K activation induced by treatment with an MEK inhibitor. Recent reports have demonstrated an MEK inhibitor-induced increase in Akt phosphorylation in BRaf-mutated cells, and have suggested the combination of MEK and PI3K inhibitors as a rational therapy for BRaf-mutated cells [14,

17]. However, these studies did not quantify phosphorylated Akt, but only showed the fold increase of pAkt in the presence and absence of MEK inhibitor. Our simulation model also indicated that the MEK inhibitor-induced fold increase in pAkt is much higher in BRaf-mutated cells than in KRas-mutated cells. Surprisingly, however, the fraction of pAkt was much lower than the fraction of pERK in BRaf-mutated cells (Fig. 9A and 9B). Thus, the fraction of pAkt did not reach a level sufficient to confer resistance to an MEK inhibitor in BRaf-mutated cells.

It is noteworthy that some FF and FB regulations included in previous models are omitted in our simulation model. Although we did not directly examine the effect of such FF and FB regulations, the readouts of FRET imaging should comprise the effect of such FF and FB regulations. Therefore, the fitted parameters in our model should include the effects of the FF and FB regulations that are not explicitly included in our simulation model. It will be beneficial to discuss some of the reported FB regulations that are not included in our model. First, ERK is known to phosphorylate and inhibit CRaf and MEK, serving as a mechanism of negative FB regulations [34, 35]. Our model is already implemented two negative FB pathways from ERK to Sos1 and EGFR. The parameters used to characterize these two negative FB pathways probably compensate the lack of negative FB regulations from ERK to CRaf and MEK. Second, it is reported that not only RSK but also ERK phosphorylates and inactivates TSC2 [36]. Again, it is likely that the effect of TSC2 inactivation by ERK is included in the parameters used to characterize TSC2 inactivation by RSK. Third, a positive FB loop from Ras-GTP to Sos have been reported by Gureasko et al [37]. Because we adopted Gureasko's parameter to describe the Sos-dependent Ras activation, our model includes the effect of this positive FB loop, even though it is not explicitly drawn in the model. Fourth, Raf kinase inhibitor protein (RKIP) is known to be phosphorylated and inactivated by ERK, thereby implementing a positive FB loop [38]. This positive FB loop should increase EGF-induced ERK phosphorylation in the early phase as does the positive FF from PI3K to Raf (Fig. 7E). Accordingly, the effect of the positive FB loop from ERK to RKIP should be included in the parameters of the FB loop of PI3K-Rac-Raf activation pathway. Finally, it has been reported that S6K and Akt phosphorylate Sin1 and, thereby, negatively regulate mTORC2 activity [39]. However, in our experimental condition, S6K activity sustains high level after EGF stimulation, indicating that the negative FB regulation to Sin1 does not play a major role in our cells (Fig. 7B, blue line).

In summary, we evaluated the quantitative contribution of FF and FB regulations

in the Ras-ERK and PI3K-S6K pathways by combining high-throughput FRET imaging with chemical inhibitor perturbations. Notably, we found a novel negative FB regulation from RSK to Raf via TSC and Rheb. Although each reaction making up the FB loop was reported previously [9, 10], the role of a negative FB loop was revealed only by the ODE-based modeling with quantitative parameters. Several issues remain to be addressed in future works. First, the kinetic parameters in the PI3K-S6K pathway should be measured experimentally to improve our mathematical model. Second, even after the fitting there remains substantial discrepancy between simulation and experimental data (Fig. 5). Our model has been developed by a bottom-up approach based on experimentally-determined parameters, and therefore it is reasonable that the model has not completely included reactions that are required for reproducing experimental data. Meanwhile, we could say that this discrepancy between simulation and experiments will provide a clue to predict hidden pathways or regulations. Nevertheless, the quantitative simulation model will have a potential advantage for predicting a rational combination of molecular targeting drugs in order to overcome their intrinsic resistance mediated by FF and FB regulations.

Materials and Methods

Reagents and plasmids

Epidermal growth factor (EGF) was purchased from Sigma-Aldrich (St. Louis, MO). PD153035, PI-103 and LY294002 were obtained from Calbiochem (La Jolla, CA). PD184352 was obtained from Toronto Research Chemicals (Ontario, Canada). BI-D1870 was purchased from Symansis (Shanghai, China). Torin1 was obtained from Tocris Bioscience (Bristol, UK). Blasticidin S and Puromycin were purchased from Invivogen (San Diego, CA). The FRET biosensors for EGFR (PicchuEV-pm), Ras (RaichuEV-Ras), ERK (EKAREV-nuc), JNK (JNKAREV), PKA (AKAR3EV) and S6K (Eevee-S6K) were developed previously [20, 40-42]. Vybrant DyeCycle Ruby was purchased from Invitrogen (San Diego, CA).

Cell culture

HeLa cells were purchased from the Human Science Research Resources Bank (Sennan-shi, Japan). HeLa cells were maintained in DMEM (Sigma-Aldrich) supplemented with 10% fetal bovine serum (FBS). Plasmids were transfected into HeLa cells by 293Fectin

(Invitrogen, Carlsbad, CA) according to the manufacturer's instructions. Stable cell lines expressing FRET biosensors were established as described previously [43].

Time-lapse FRET imaging

FRET imaging were performed as described previously [43]. For multiplex imaging, HeLa cells stably expressing FRET biosensors were mixed and passaged into 8 wells of a 96-well glass base plate or 4-well glass-bottom dish. One day after seeding, the cells were serum starved for one day with the medium described above. The glass-bottom 96-well plate or 4-well dish base plate was imaged by an inverted microscope as described earlier. The imaging interval was three minutes with 96-well glass base plate and one or two minutes with 4-well glass-bottom dish (Supplementary dataset 1). After the time-lapse imaging, the nuclei of the cells were stained by Vybrant DyeCycle Ruby and imaged. Using the nucleus-stained images, the FRET images were processed and analyzed with a custom-made MATLAB program as described below.

Image processing with a custom-made MATLAB program

The custom-made image-processing program was developed with MATLAB software (version R2012a; The Mathworks Inc., Natick, MA). This program recognized cell nuclei from images of nuclei stained with Vybrant DyeCycle Ruby. To distinguish 3 cell lines mixed as described above, it executed an algorithm to classify them according to their fluorescent localization. Then, the FRET and CFP intensities were averaged over each cell area, and the FRET/CFP value was calculated. In some experiments, the FRET/CFP value from before 10 min to the time of stimulation was averaged and used as the reference. The ratio of the raw FRET/CFP value to the reference value was defined as the normalized FRET/CFP value. In the experiment in Fig. 8B, this program recognized cells from fluorescent images of EKAREV-nuc and counted the cell number.

Numerical simulation of EKAREV-nuc

Numerical simulation of EKAREV-nuc was performed by MATLAB software to convert the amount of phosphorylated ERK into FRET/CFP values in EKAREV-nuc (Supplementary Codes). FRET/CFP value was calculated by the following expression.

$$FRET/CFP\_value = \frac{[pEKAR\_folded]}{[EKAR]+[EKAR\_pTpYERK]+[pEKAR]}$$

Kinetic modeling and numerical simulation

The Ras/ERK and Akt pathways simulation implemented here consists of 48 kinetic reactions involving 19 different molecules, 73 parameters and 4 inhibitor values. The kinetic reactions were based on Michaelis-Menten kinetics, but many reactions were described as the first-order kinetics when reactions could be approximated in order to decrease the number of parameters. The biochemical reactions and the parameters used in this study are shown in the Supporting Information (Table S1-S3). All kinetic reactions were described with mass action kinetics by using CellDesigner (version 4.1) [44] (Fig. 4). The ordinary differential equations with parameters were exported to the MATLAB software through a Systems Biology Workbench (version 2.8.1) [45]. Numerical simulation was performed by MATLAB software (Supplementary Codes). The reactions with inhibitors were expressed as follows.

$$\frac{\mathrm{d[Product]}}{\mathrm{dt}} = \mathrm{Reaction\_rate} * \mathrm{[Kinase]} * \mathrm{[Substrate]} * \mathrm{inhibitor\_value}$$

When the simulation was performed without inhibitors, the inhibitor value was set to 1. When inhibitors were introduced in the simulation, the inhibitor value was set from 0 to 1. The inhibition strength in Fig. 8 and Fig. 9 was converted to an inhibitor value according to the following Hill equation:

$$inhibitor\_value = 0.01 + \frac{0.99 * 0.4^5}{(inhibition\_strength)^5 + 0.4^5}$$

where each constant is determined so as to reproduce the experimental result.

Parameter fitting

For the determination of kinetic parameters, unconstrained nonlinear optimization was implemented by MATLAB software using the fminsearch function. To compare the results of simulation and FRET imaging, FRET ratios were estimated by fractions of phosphorylated molecules in the simulation result.

Acknowledgements

We are grateful to the members of the Matsuda Laboratory for their helpful input. We also thank K. Ui-Tei for the shRNA plasmids. Y. Inaoka, K. Hirano, A. Katsumata, N. Nonaka,

and A. Kawagishi are also to be thanked for their technical assistance. KA and MM were supported by the Research Program of Innovative Cell Biology by Innovative Technology (Cell Innovation) and Platform for Dynamic Approaches to Living System from the Ministry of Education, Culture, Sports, and Science, Japan. KA was supported by a Grant-in-Aid for Young Scientists (B) (23701052). NK and YF were supported by a Grant-in-Aid for JSPS Fellows.

Author Contributions

Y.F., K.A. and M.M. designed the experiments and wrote the paper. Y.F. and N.K. conducted the experiments. Y.F. analyzed the data and performed the modeling and simulation.

References

1. Chang, L. & Karin, M. (2001) Mammalian MAP kinase signalling cascades, *Nature.* **410**, 37-40.
2. Qi, M. & Elion, E. A. (2005) MAP kinase pathways, *J Cell Sci.* **118**, 3569-72.
3. Katso, R., Okkenhaug, K., Ahmadi, K., White, S., Timms, J. & Waterfield, M. D. (2001) Cellular function of phosphoinositide 3-kinases: implications for development, homeostasis, and cancer, *Annu Rev Cell Dev Biol.* **17**, 615-75.
4. Vogelstein, B., Papadopoulos, N., Velculescu, V. E., Zhou, S., Diaz, L. A., Jr. & Kinzler, K. W. (2013) Cancer genome landscapes, *Science.* **339**, 1546-58.
5. Barretina, J., Caponigro, G., Stransky, N., Venkatesan, K., Margolin, A. A., Kim, S., Wilson, C. J., Lehar, J., Kryukov, G. V., Sonkin, D., Reddy, A., Liu, M., Murray, L., Berger, M. F., Monahan, J. E., Morais, P., Meltzer, J., Korejwa, A., Jane-Valbuena, J., Mapa, F. A., Thibault, J., Bric-Furlong, E., Raman, P., Shipway, A., Engels, I. H., Cheng, J., Yu, G. K., Yu, J., Aspesi, P., Jr., de Silva, M., Jagtap, K., Jones, M. D., Wang, L., Hatton, C., Palescandolo, E., Gupta, S., Mahan, S., Sougnez, C., Onofrio, R. C., Liefeld, T., MacConaill, L., Winckler, W., Reich, M., Li, N., Mesirov, J. P., Gabriel, S. B., Getz, G., Ardlie, K., Chan, V., Myer, V. E., Weber, B. L., Porter, J., Warmuth, M., Finan, P., Harris, J. L., Meyerson, M., Golub, T. R., Morrissey, M. P., Sellers, W. R., Schlegel, R. & Garraway, L. A. (2012) The Cancer Cell Line Encyclopedia enables predictive modelling of anticancer drug sensitivity, *Nature.* **483**, 603-7.

6. Hanahan, D. & Weinberg, R. A. (2011) Hallmarks of cancer: the next generation, *Cell.* **144**, 646-74.
7. Avraham, R. & Yarden, Y. (2011) Feedback regulation of EGFR signalling: decision making by early and delayed loops, *Nat Rev Mol Cell Biol.* **12**, 104-17.
8. Waters, S. B., Chen, D., Kao, A. W., Okada, S., Holt, K. H. & Pessin, J. E. (1996) Insulin and epidermal growth factor receptors regulate distinct pools of Grb2-SOS in the control of Ras activation, *J Biol Chem.* **271**, 18224-30.
9. Roux, P. P., Ballif, B. A., Anjum, R., Gygi, S. P. & Blenis, J. (2004) Tumor-promoting phorbol esters and activated Ras inactivate the tuberous sclerosis tumor suppressor complex via p90 ribosomal S6 kinase, *Proc Natl Acad Sci U S A.* **101**, 13489-94.
10. Karbowniczek, M., Robertson, G. P. & Henske, E. P. (2006) Rheb inhibits C-raf activity and B-raf/C-raf heterodimerization, *J Biol Chem.* **281**, 25447-56.
11. Aksamitiene, E., Achanta, S., Kolch, W., Kholodenko, B. N., Hoek, J. B. & Kiyatkin, A. (2011) Prolactin-stimulated activation of ERK1/2 mitogen-activated protein kinases is controlled by PI3-kinase/Rac/PAK signaling pathway in breast cancer cells, *Cell Signal.* **23**, 1794-805.
12. Turke, A. B., Song, Y., Costa, C., Cook, R., Arteaga, C. L., Asara, J. M. & Engelman, J. A. (2012) MEK inhibition leads to PI3K/AKT activation by relieving a negative feedback on ERBB receptors, *Cancer Res.* **72**, 3228-37.
13. Friday, B. B., Yu, C., Dy, G. K., Smith, P. D., Wang, L., Thibodeau, S. N. & Adjei, A. A. (2008) BRAF V600E disrupts AZD6244-induced abrogation of negative feedback pathways between extracellular signal-regulated kinase and Raf proteins, *Cancer Res.* **68**, 6145-53.
14. Won, J. K., Yang, H. W., Shin, S. Y., Lee, J. H., Heo, W. D. & Cho, K. H. (2012) The crossregulation between ERK and PI3K signaling pathways determines the tumoricidal efficacy of MEK inhibitor, *J Mol Cell Biol.* **4**, 153-63.
15. Prahallad, A., Sun, C., Huang, S., Di Nicolantonio, F., Salazar, R., Zecchin, D., Beijersbergen, R. L., Bardelli, A. & Bernards, R. (2012) Unresponsiveness of colon cancer to BRAF(V600E) inhibition through feedback activation of EGFR, *Nature.* **483**, 100-3.
16. Cirit, M., Wang, C. C. & Haugh, J. M. (2010) Systematic quantification of negative feedback mechanisms in the extracellular signal-regulated kinase (ERK) signaling network, *J Biol Chem.* **285**, 36736-44.
17. Klinger, B., Sieber, A., Fritsche-Guenther, R., Witzel, F., Berry, L., Schumacher, D., Yan, Y., Durek, P., Merchant, M., Schafer, R., Sers, C. & Bluthgen, N. (2013) Network

quantification of EGFR signaling unveils potential for targeted combination therapy, *Mol Syst Biol.* **9**, 673.
18. Inoue, T. & Meyer, T. (2008) Synthetic activation of endogenous PI3K and Rac identifies an AND-gate switch for cell polarization and migration, *PLoS One.* **3**, e3068.
19. Jares-Erijman, E. A. & Jovin, T. M. (2003) FRET imaging, *Nat Biotechnol.* **21**, 1387-95.
20. Komatsu, N., Aoki, K., Yamada, M., Yukinaga, H., Fujita, Y., Kamioka, Y. & Matsuda, M. (2011) Development of an optimized backbone of FRET biosensors for kinases and GTPases, *Mol Biol Cell.* **22**, 4647-56.
21. Kamioka, Y., Yasuda, S., Fujita, Y., Aoki, K. & Matsuda, M. (2010) Multiple decisive phosphorylation sites for the negative feedback regulation of SOS1 via ERK, *J Biol Chem.* **285**, 33540-8.
22. Sato, K., Shin, M. S., Sakimura, A., Zhou, Y., Tanaka, T., Kawanishi, M., Kawasaki, Y., Yokoyama, S., Koizumi, K., Saiki, I. & Sakurai, H. (2013) Inverse correlation between Thr-669 and constitutive tyrosine phosphorylation in the asymmetric EGFR dimer conformation, *Cancer Sci*.
23. Yang, H. W., Shin, M. G., Lee, S., Kim, J. R., Park, W. S., Cho, K. H., Meyer, T. & Do Heo, W. (2012) Cooperative activation of PI3K by Ras and Rho family small GTPases, *Mol Cell.* **47**, 281-90.
24. Sapkota, G. P., Cummings, L., Newell, F. S., Armstrong, C., Bain, J., Frodin, M., Grauert, M., Hoffmann, M., Schnapp, G., Steegmaier, M., Cohen, P. & Alessi, D. R. (2007) BI-D1870 is a specific inhibitor of the p90 RSK (ribosomal S6 kinase) isoforms in vitro and in vivo, *Biochem J.* **401**, 29-38.
25. Ma, W., Trusina, A., El-Samad, H., Lim, W. A. & Tang, C. (2009) Defining network topologies that can achieve biochemical adaptation, *Cell.* **138**, 760-73.
26. Garnett, M. J., Edelman, E. J., Heidorn, S. J., Greenman, C. D., Dastur, A., Lau, K. W., Greninger, P., Thompson, I. R., Luo, X., Soares, J., Liu, Q., Iorio, F., Surdez, D., Chen, L., Milano, R. J., Bignell, G. R., Tam, A. T., Davies, H., Stevenson, J. A., Barthorpe, S., Lutz, S. R., Kogera, F., Lawrence, K., McLaren-Douglas, A., Mitropoulos, X., Mironenko, T., Thi, H., Richardson, L., Zhou, W., Jewitt, F., Zhang, T., O'Brien, P., Boisvert, J. L., Price, S., Hur, W., Yang, W., Deng, X., Butler, A., Choi, H. G., Chang, J. W., Baselga, J., Stamenkovic, I., Engelman, J. A., Sharma, S. V., Delattre, O., Saez-Rodriguez, J., Gray, N. S., Settleman, J., Futreal, P. A., Haber, D. A., Stratton, M. R., Ramaswamy, S., McDermott, U. & Benes, C. H. (2012) Systematic identification of genomic markers of drug sensitivity

in cancer cells, *Nature.* **483**, 570-5.
27. Santos, S. D., Verveer, P. J. & Bastiaens, P. I. (2007) Growth factor-induced MAPK network topology shapes Erk response determining PC-12 cell fate, *Nat Cell Biol.* **9**, 324-30.
28. Poulikakos, P. I., Persaud, Y., Janakiraman, M., Kong, X., Ng, C., Moriceau, G., Shi, H., Atefi, M., Titz, B., Gabay, M. T., Salton, M., Dahlman, K. B., Tadi, M., Wargo, J. A., Flaherty, K. T., Kelley, M. C., Misteli, T., Chapman, P. B., Sosman, J. A., Graeber, T. G., Ribas, A., Lo, R. S., Rosen, N. & Solit, D. B. (2011) RAF inhibitor resistance is mediated by dimerization of aberrantly spliced BRAF(V600E), *Nature.* **480**, 387-90.
29. Shi, H., Moriceau, G., Kong, X., Lee, M. K., Lee, H., Koya, R. C., Ng, C., Chodon, T., Scolyer, R. A., Dahlman, K. B., Sosman, J. A., Kefford, R. F., Long, G. V., Nelson, S. F., Ribas, A. & Lo, R. S. (2012) Melanoma whole-exome sequencing identifies (V600E)B-RAF amplification-mediated acquired B-RAF inhibitor resistance, *Nat Commun.* **3**, 724.
30. Wilson, T. R., Fridlyand, J., Yan, Y., Penuel, E., Burton, L., Chan, E., Peng, J., Lin, E., Wang, Y., Sosman, J., Ribas, A., Li, J., Moffat, J., Sutherlin, D. P., Koeppen, H., Merchant, M., Neve, R. & Settleman, J. (2012) Widespread potential for growth-factor-driven resistance to anticancer kinase inhibitors, *Nature.* **487**, 505-9.
31. Straussman, R., Morikawa, T., Shee, K., Barzily-Rokni, M., Qian, Z. R., Du, J., Davis, A., Mongare, M. M., Gould, J., Frederick, D. T., Cooper, Z. A., Chapman, P. B., Solit, D. B., Ribas, A., Lo, R. S., Flaherty, K. T., Ogino, S., Wargo, J. A. & Golub, T. R. (2012) Tumour micro-environment elicits innate resistance to RAF inhibitors through HGF secretion, *Nature.* **487**, 500-4.
32. Solit, D. B., Garraway, L. A., Pratilas, C. A., Sawai, A., Getz, G., Basso, A., Ye, Q., Lobo, J. M., She, Y., Osman, I., Golub, T. R., Sebolt-Leopold, J., Sellers, W. R. & Rosen, N. (2006) BRAF mutation predicts sensitivity to MEK inhibition, *Nature.* **439**, 358-62.
33. Engelman, J. A., Chen, L., Tan, X., Crosby, K., Guimaraes, A. R., Upadhyay, R., Maira, M., McNamara, K., Perera, S. A., Song, Y., Chirieac, L. R., Kaur, R., Lightbown, A., Simendinger, J., Li, T., Padera, R. F., Garcia-Echeverria, C., Weissleder, R., Mahmood, U., Cantley, L. C. & Wong, K. K. (2008) Effective use of PI3K and MEK inhibitors to treat mutant Kras G12D and PIK3CA H1047R murine lung cancers, *Nat Med.* **14**, 1351-6.
34. Brunet, A., Pages, G. & Pouyssegur, J. (1994) Growth factor-stimulated MAP kinase induces rapid retrophosphorylation and inhibition of MAP kinase kinase (MEK1), *FEBS Lett.* **346**, 299-303.
35. Dougherty, M. K., Muller, J., Ritt, D. A., Zhou, M., Zhou, X. Z., Copeland, T. D.,

Conrads, T. P., Veenstra, T. D., Lu, K. P. & Morrison, D. K. (2005) Regulation of Raf-1 by direct feedback phosphorylation, *Mol Cell.* **17**, 215-24.
36. Ma, L., Chen, Z., Erdjument-Bromage, H., Tempst, P. & Pandolfi, P. P. (2005) Phosphorylation and functional inactivation of TSC2 by Erk implications for tuberous sclerosis and cancer pathogenesis, *Cell.* **121**, 179-93.
37. Gureasko, J., Galush, W. J., Boykevisch, S., Sondermann, H., Bar-Sagi, D., Groves, J. T. & Kuriyan, J. (2008) Membrane-dependent signal integration by the Ras activator Son of sevenless, *Nat Struct Mol Biol.* **15**, 452-61.
38. Shin, S. Y., Rath, O., Choo, S. M., Fee, F., McFerran, B., Kolch, W. & Cho, K. H. (2009) Positive- and negative-feedback regulations coordinate the dynamic behavior of the Ras-Raf-MEK-ERK signal transduction pathway, *J Cell Sci.* **122**, 425-35.
39. Liu, P., Gan, W., Inuzuka, H., Lazorchak, A. S., Gao, D., Arojo, O., Liu, D., Wan, L., Zhai, B., Yu, Y., Yuan, M., Kim, B. M., Shaik, S., Menon, S., Gygi, S. P., Lee, T. H., Asara, J. M., Manning, B. D., Blenis, J., Su, B. & Wei, W. (2013) Sin1 phosphorylation impairs mTORC2 complex integrity and inhibits downstream Akt signalling to suppress tumorigenesis, *Nat Cell Biol.* **15**, 1340-50.
40. Mochizuki, N., Yamashita, S., Kurokawa, K., Ohba, Y., Nagai, T., Miyawaki, A. & Matsuda, M. (2001) Spatio-temporal images of growth-factor-induced activation of Ras and Rap1, *Nature.* **411**, 1065-8.
41. Kurokawa, K., Mochizuki, N., Ohba, Y., Mizuno, H., Miyawaki, A. & Matsuda, M. (2001) A pair of fluorescent resonance energy transfer-based probes for tyrosine phosphorylation of the CrkII adaptor protein in vivo, *J Biol Chem.* **276**, 31305-10.
42. Harvey, C. D., Ehrhardt, A. G., Cellurale, C., Zhong, H., Yasuda, R., Davis, R. J. & Svoboda, K. (2008) A genetically encoded fluorescent sensor of ERK activity, *Proc Natl Acad Sci U S A.* **105**, 19264-9.
43. Aoki, K., Komatsu, N., Hirata, E., Kamioka, Y. & Matsuda, M. (2012) Stable expression of FRET biosensors: a new light in cancer research, *Cancer Sci.* **103**, 614-9.
44. Kitano, H., Funahashi, A., Matsuoka, Y. & Oda, K. (2005) Using process diagrams for the graphical representation of biological networks, *Nat Biotechnol.* **23**, 961-6.
45. Sauro, H. M., Hucka, M., Finney, A., Wellock, C., Bolouri, H., Doyle, J. & Kitano, H. (2003) Next generation simulation tools: the Systems Biology Workbench and BioSPICE integration, *OMICS.* **7**, 355-72.
46. Aoki, K., Kumagai, Y., Sakurai, A., Komatsu, N., Fujita, Y., Shionyu, C. & Matsuda, M. (2013) Stochastic ERK Activation Induced by Noise and Cell-to-Cell Propagation

Regulates Cell Density-Dependent Proliferation, *Mol Cell*.

Supporting information

The following supplementary material is available at the publisher's web site:
Table S1. The initial concentration of signaling molecules in simulation.
Table S2. Kinetic reactions and parameters.
Table S3. The inhibitor value in simulation.
Supplementary Dataset 1. The large scale time-course data of change in EGFR, Ras, ERK, JNK, PKA and S6K activity upon EGF stimulation in combination with chemical inhibitors and compounds.
Supplementary Dataset 2. Pharmacological profiling data extracted from Mathew J. Garnett et al. Nature 2012.
Supplementary Codes. MATLAB .m files of the Ras/ERK and Akt pathways model and numerical simulation.

Figure legend

Figure 1. Outline of FRET imaging, image processing, and kinetic simulation. HeLa cells stably expressing FRET biosensors for Ras (RaichuEV-Ras-pm), EGFR (PicchuEV-pm), ERK (EKAREV-nls), JNK (JNKAREV-nls), S6K (Eevee-S6K-nes) and PKA (AKAR3EV-nes) were established. Three cell lines (grey rectangles) were mixed and seeded onto 96-well or 4-well glass-bottom dishes. The cells were stimulated with EGF and inhibitors, and imaged with an inverted epifluorescence microscope. The images were processed by a semi-automatic program to extract changes in molecular activity. Based on a large imaging data set and kinetic parameters, a kinetic simulation model was built and compared with experimental data.

Figure 2. Sensitivity of PicchuEV-pm and EKAREV-nuc. (**A** and **B**) HeLa cells stably expressing PicchuEV-pm (A) and EKAREV-nuc (B) were serum starved and time lapse images were obtained. While FRET imaging, cells were stimulated with 50 ng/ml EGF and treated with 1 μM PD153035, an EGFR inhibitor (A) or 10 μM PD184352, a MEK inhibitor (B) at time points indicated in each graph. Dark lines represent the average value

with areas reflecting the s.d. (n > 9). (**C**) HeLa cells stably expressing EKAREV-nuc were stimulated with various concentrations of TPA. The FRET/CFP values were quantified at 30 min after TPA stimulation. Under the same condition, HeLa cells were lysed with SDS sample buffer and subjected to Phos-Tag Western blotting in order to quantify the fraction of phosphorylated ERK (pTpY-ERK). FRET/CFP values are plotted as a function of the fractions of pTpY-ERK (dots) and fitted by computer simulation (line). Of note, experimental data are reused from [46]. (**D**) Schematic of the simulation model of EKAREV-nuc used in (C). FRET/CFP value was calculated as described in Materials and Methods.

Figure 3. Evidences of feedforward and feedback regulations in EGFR signaling. (**A**) Schematic of the negative feedback from ERK to EGFR. (**B**) EGFR activity upon 10 ng/ml EGF before or after inhibitor treatments (20 μM LY294002, a PI3K inhibitor; 10 μM PD184352, an MEK inhibitor; 1 μM PD153035, an EGFR inhibitor). The FRET/CFP values are normalized by the FRET/CFP value just before inhibitor treatment. (**C**) Schematic of the coherent feedforward regulation from Ras to Raf through PI3K and Rac1. (**D**) ERK activity in response to 10 ng/ml EGF, followed by the treatment with inhibitors at the indicated time points (10 μM PI-103, a PI3K inhibitor, 10 μM PD184352, and 1 μM PD153035). The FRET/CFP values are normalized by the FRET/CFP value just before inhibitor treatment. (**E** and **F**) The dominant negative mutant of Rac1(RacN17 (E)), and HRas (HRasN17 (F)), reduced 50 ng/ml EGF-induced ERK and S6K activation, respectively. (**G**) Schematic of the negative feedback from RSK to Raf through TSC and Rheb. (**H** and **I**) ERK (H) and S6K (I) activity upon inhibitors (1 μM Torin1, an mTORC1/2 inhibtor; 10 μM BI-D1870, a RSK inhibitor) and 10 ng/ml EGF treatment. (**J**) Rheb depletion by shRNA enhanced the ERK activation induced by 1 μM BI-D1870 treatment. Dark lines represent the average value with areas reflecting the s.d. (n > 9).

Figure 4. Overview of the kinetic simulation model of Ras-ERK and PI3K-S6K pathways. Diagram of the kinetic simulation model of the Ras-ERK and PI3K-S6K signaling network is depicted with gene mutations and molecular targeting drugs. All parameters and reactions are described in Table S1-3.

Figure 5. Simulated ERK activities with experimental results. (**A**-**D**) ERK activity in response to 10 ng/ml EGF, followed by the treatment with mock (A) or inhibitors at the

indicated time points. Circles represent averaged FRET/CFP values as in Fig. 3D (n > 9). The FRET/CFP values are normalized by the FRET/CFP value just before inhibitor treatment. Solid lines demonstrate reconstituted FRET/CFP values from simulated active ERK value according to the model shown in Fig. 2C and 2D. (**E**) EGF-induced ERK activation with or without Rac1 dominant negative mutant (Rac1N17). Circles represent averaged FRET/CFP values as in Fig. 3E (n > 9). (**F**) ERK activity upon inhibitors (10 μM BI-D1870, a RSK inhibitor) and 10 ng/ml EGF treatment. Circles represent averaged FRET/CFP values as in Fig. 3H (n > 9).

Figure 6. Kinetic simulation of Ras-ERK and PI3K-S6K signaling including feedforward and feedback regulations. (**A**) Schematic representation of EGFR signaling including Ras-ERK and PI3K-S6K pathways. (**B**) Numerical simulation of EGFR (left) and ERK (right) activity in response to EGF and the indicated inhibitors. (**C** and **D**) Rac1 (C) and Ras (D) inhibition markedly reduced the ERK and S6K activation stimulated by EGF, respectively. (**E**) Simulation of ERK (left) and S6K (right) activity in response to the indicated inhibitors and EGF. (**F**) Rheb inhibition enhanced the ERK activation induced by an RSK inhibitor.

Figure 7. Coordinated roles of feedforward and feedback regulations. (**A**) Simulation of S6K activity upon EGF followed by inhibitor treatment. (**B**) S6K activity upon 50 ng/ml EGF followed by inhibitor treatment (20 μM LY294002, 10 μM PD184352, and 1 μM PD153035). (**C** and **D**) Pretreatment with an RSK inhibitor reduced the EGF-induced ERK activation in both the simulation (C) and experiments (D), in which cells were treated with 10 μM BI-D1870, followed by stimulation with 1 ng/ml EGF. (**E**) Simulation of ERK activation induced by EGF under the condition that the indicated feedforward or feedback regulations are impaired. Dark lines represent the average value with areas reflecting the s.d. (n > 9). (**F**) Schematic of the roles of feedforward and feedback regulations in a manner dependent on the temporal phase of EGF stimulation.

Figure 8. Evaluation of the effect of molecular targeting drugs on cytotoxicity in KRas- or BRaf-mutated cells. (**A**) Pharmacological profiling data obtained from the Cancer Cell Line Encyclopedia. The average dose-responses of cancer cell lines against a BRaf inhibitor, PLX-4720, and an MEK inhibitor, AZD6244, are shown. The numbers of cell lines are as follows: KRas mutant, n = 82; BRaf mutant, n = 50. (**B**) HCT-116 cells and

HT-29 cells were treated with PI-103 in the absence (left) or presence (right) of AZD6244. Three days after treatment, the cell number was quantified. Equal concentrations of both AZD6244 and PI-103 were administered in the concomitant treatment. The average values of 5 experiments are shown. Error bars indicate the S.D. (**C**) The sums of the absolute values of pERK and pAkt under the conditions of BRaf inhibition (left), MEK inhibition (middle left), PI3K inhibition (middle right) and concomitant inhibition of both MEK and PI3K (right) were numerically calculated, and normalized at non-inhibition condition in KRas- or BRaf-mutated cells. MEK and PI3K were equally inhibited under the concomitant inhibition of MEK and PI3K (right).

Figure 9. Relation between feedforward/feedback regulations and differential effects of molecular targeting drugs on mutant cells. (**A** and **B**) Dose response of ERK (left) and Akt (right) phosphorylation to MEK inhibition (cyan), BRaf inhibition (orange), PI3K inhibition (green) and concomitant inhibition of both MEK and PI3K (magenta) in KRas-mutated (A) and BRaf-mutated (B) cells. (**C**) Proposed model of the differential effects of molecular targeting drugs on KRas-mutated and BRaf-mutated cells.

Figure 1

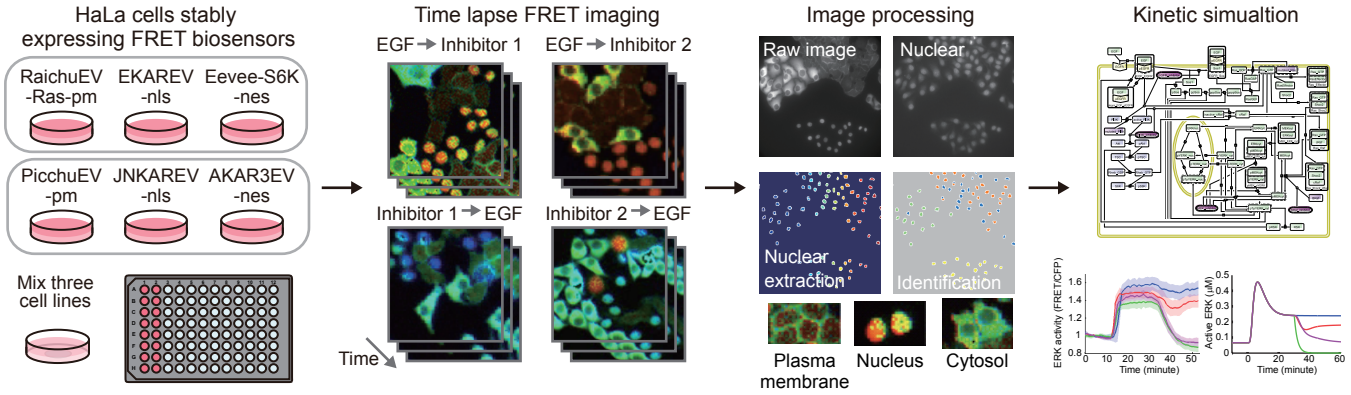
HaLa cells stably expressing FRET biosensors
RaichuEV -Ras-pm
EKAREV -nls
Eevee-S6K -nes
PicchuEV -pm
JNKAREV -nls
AKAR3EV -nes
Mix three cell lines
Time lapse FRET imaging
EGF → Inhibitor 1
EGF → Inhibitor 2
Inhibitor 1 → EGF
Inhibitor 2 → EGF
Time
Image processing
Raw image
Nuclear
Nuclear extraction
Identification
Plasma membrane
Nucleus
Cytosol
Kinetic simualtion
ERK activity (FRET/CFP)
Time (minute)
Active ERK (μM)
Time (minute)

Figure 2

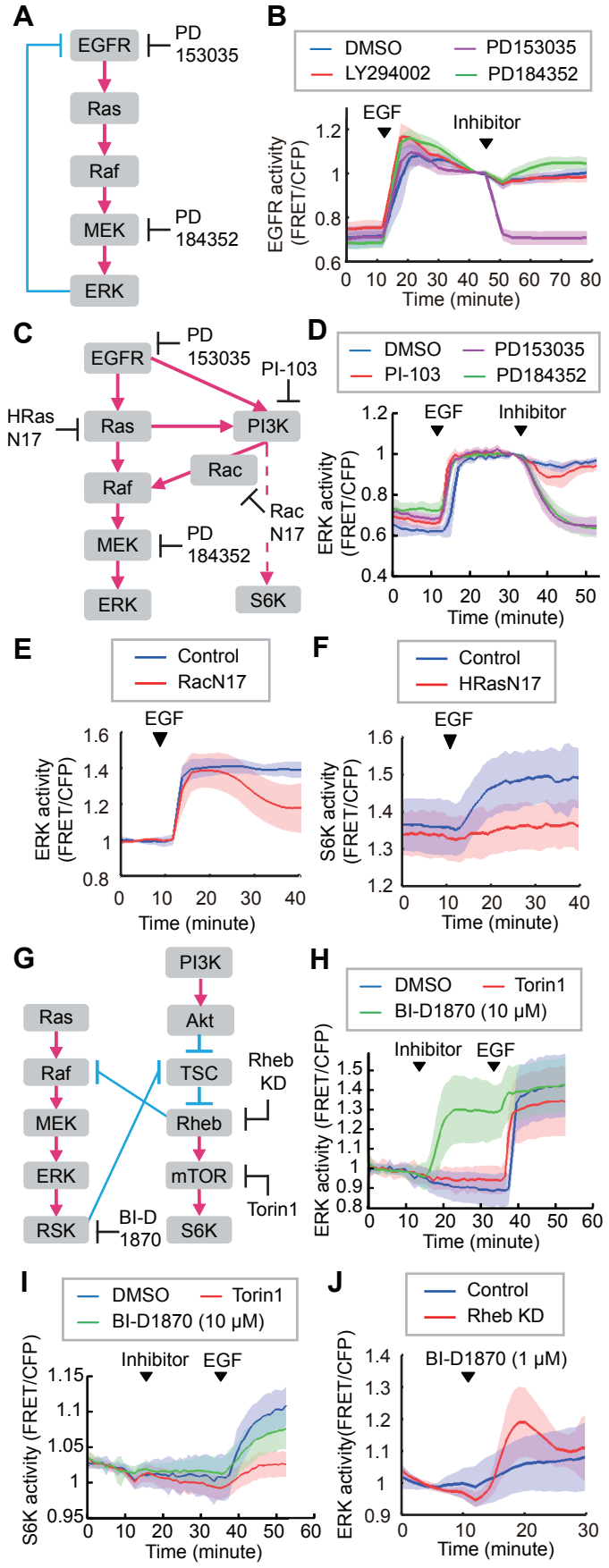
A
EGFR
PD 153035
Ras
Raf
MEK
PD 184352
ERK
B
DMSO
LY294002
PD153035
PD184352
EGF
Inhibitor
EGFR activity (FRET/CFP)
Time (minute)
C
EGFR
PD 153035
PI-103
HRas N17
Ras
PI3K
Rac
Raf
Rac N17
MEK
PD 184352
ERK
S6K
D
DMSO
PI-103
PD153035
PD184352
EGF
Inhibitor
ERK activity (FRET/CFP)
Time (minute)
E
Control
RacN17
EGF
ERK activity (FRET/CFP)
Time (minute)
F
Control
HRasN17
EGF
S6K activity (FRET/CFP)
Time (minute)
G
PI3K
Ras
Akt
Raf
TSC
Rheb KD
MEK
Rheb
ERK
mTOR
Torin1
RSK
BI-D 1870
S6K
H
DMSO
Torin1
BI-D1870 (10 μM)
Inhibitor
EGF
ERK activity (FRET/CFP)
Time (minute)
I
DMSO
Torin1
BI-D1870 (10 μM)
Inhibitor
EGF
S6K activity (FRET/CFP)
Time (minute)
J
Control
Rheb KD
BI-D1870 (1 μM)
ERK activity(FRET/CFP)
Time (minute)

Figure 3

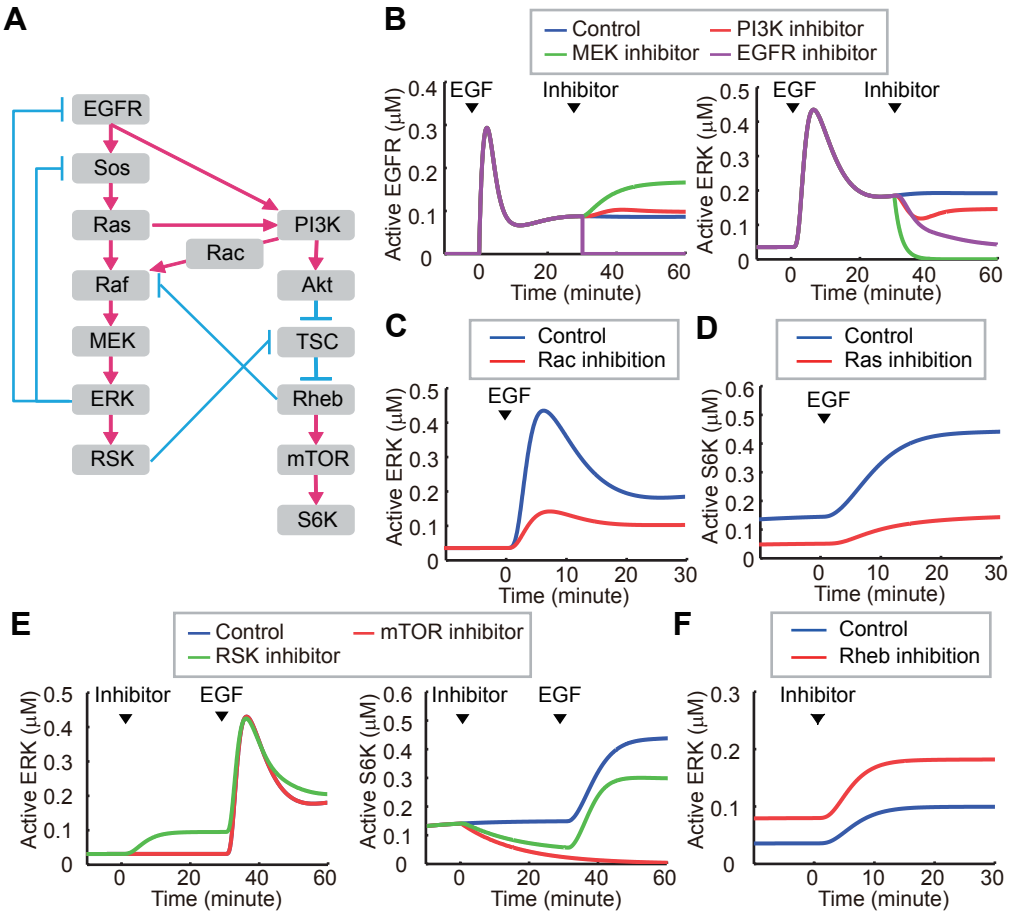
A
EGFR
Sos
Ras
Raf
MEK
ERK
RSK
PI3K
Rac
Akt
TSC
Rheb
mTOR
S6K
B
Control
PI3K inhibitor
MEK inhibitor
EGFR inhibitor
Active EGFR (μM)
Active ERK (μM)
EGF
Inhibitor
Time (minute)
C
Control
Rac inhibition
Active ERK (μM)
EGF
Time (minute)
D
Control
Ras inhibition
Active S6K (μM)
EGF
Time (minute)
E
Control
mTOR inhibitor
RSK inhibitor
Active ERK (μM)
Active S6K (μM)
Inhibitor
EGF
Time (minute)
F
Control
Rheb inhibition
Active ERK (μM)
Inhibitor
Time (minute)

Figure 4

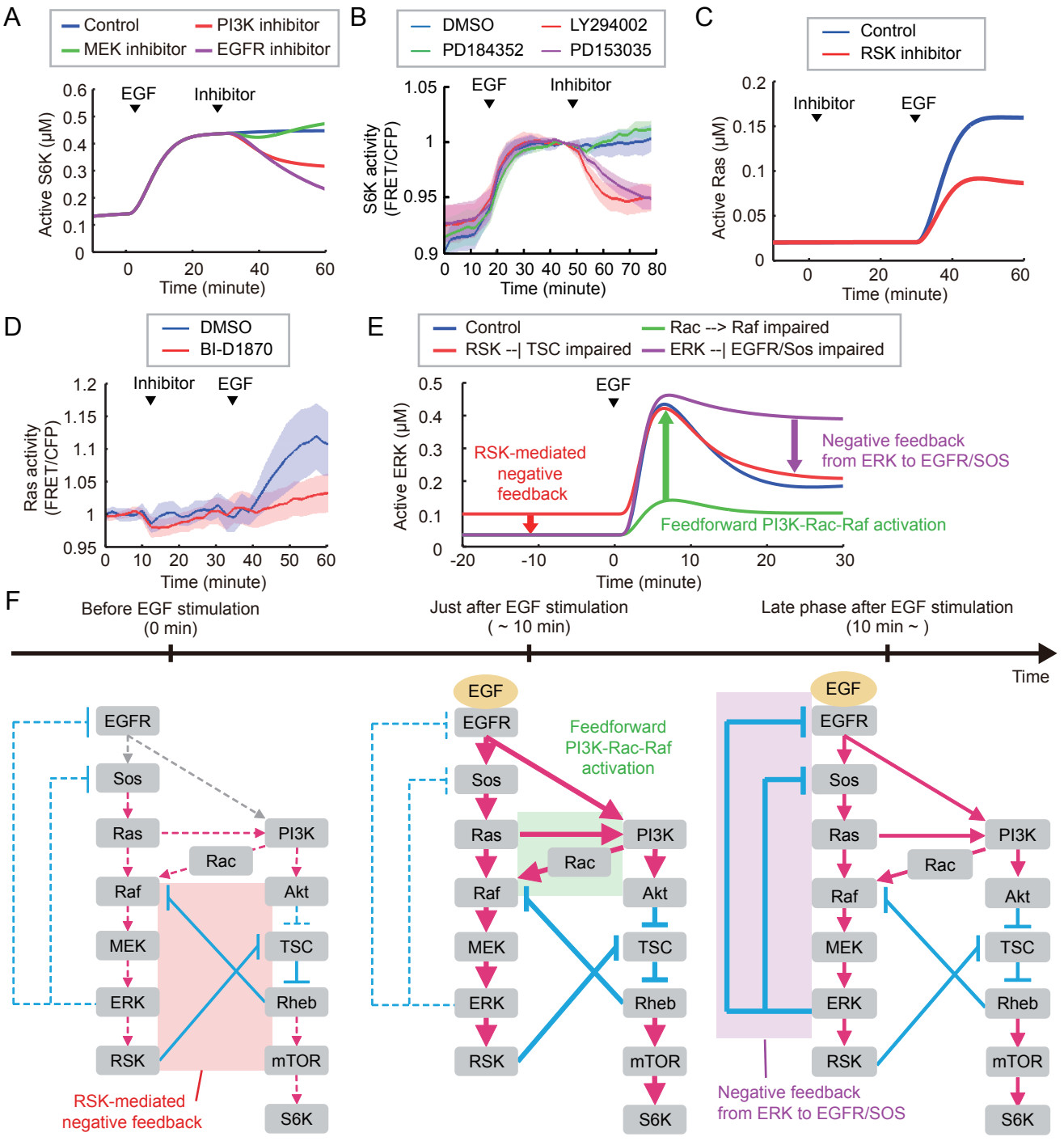
A
Control
PI3K inhibitor
MEK inhibitor
EGFR inhibitor
Active S6K (μM)
EGF
Inhibitor
Time (minute)
B
DMSO
LY294002
PD184352
PD153035
S6K activity (FRET/CFP)
EGF
Inhibitor
Time (minute)
C
Control
RSK inhibitor
Active Ras (μM)
Inhibitor
EGF
Time (minute)
D
DMSO
BI-D1870
Ras activity (FRET/CFP)
Inhibitor
EGF
Time (minute)
E
Control
RSK --| TSC impaired
Rac --> Raf impaired
ERK --| EGFR/Sos impaired
Active ERK (μM)
EGF
RSK-mediated negative feedback
Negative feedback from ERK to EGFR/SOS
Feedforward PI3K-Rac-Raf activation
Time (minute)
F
Before EGF stimulation (0 min)
Just after EGF stimulation (~ 10 min)
Late phase after EGF stimulation (10 min ~)
Time
EGF
EGFR
Sos
Ras
PI3K
Rac
Raf
Akt
MEK
TSC
ERK
Rheb
RSK
mTOR
S6K
RSK-mediated negative feedback
Feedforward PI3K-Rac-Raf activation
Negative feedback from ERK to EGFR/SOS

Figure 5

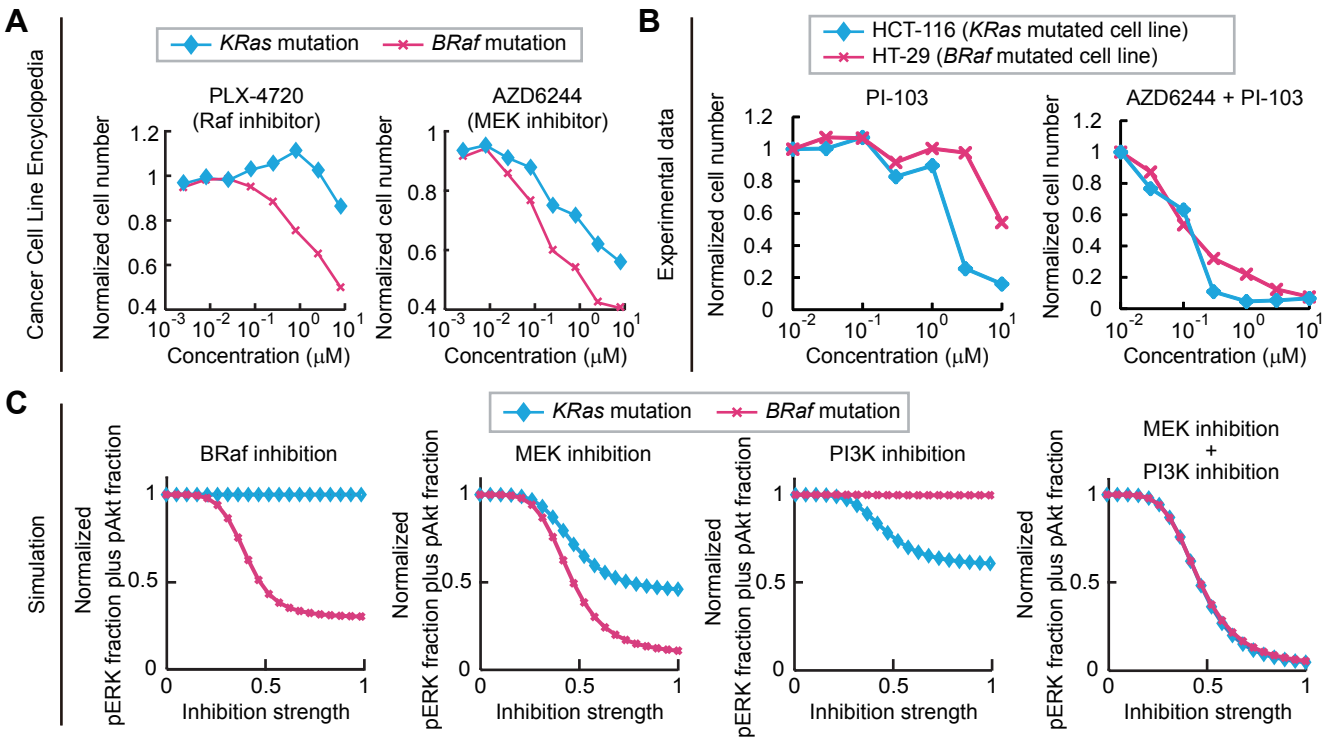
A
Cancer Cell Line Encyclopedia
KRas mutation
BRaf mutation
PLX-4720
(Raf inhibitor)
AZD6244
(MEK inhibitor)
Normalized cell number
Concentration (μM)
B
Experimental data
HCT-116 (KRas mutated cell line)
HT-29 (BRaf mutated cell line)
PI-103
AZD6244 + PI-103
C
Simulation
BRaf inhibition
MEK inhibition
PI3K inhibition
MEK inhibition
+
PI3K inhibition
Normalized
pERK fraction plus pAkt fraction
Inhibition strength

Figure 6

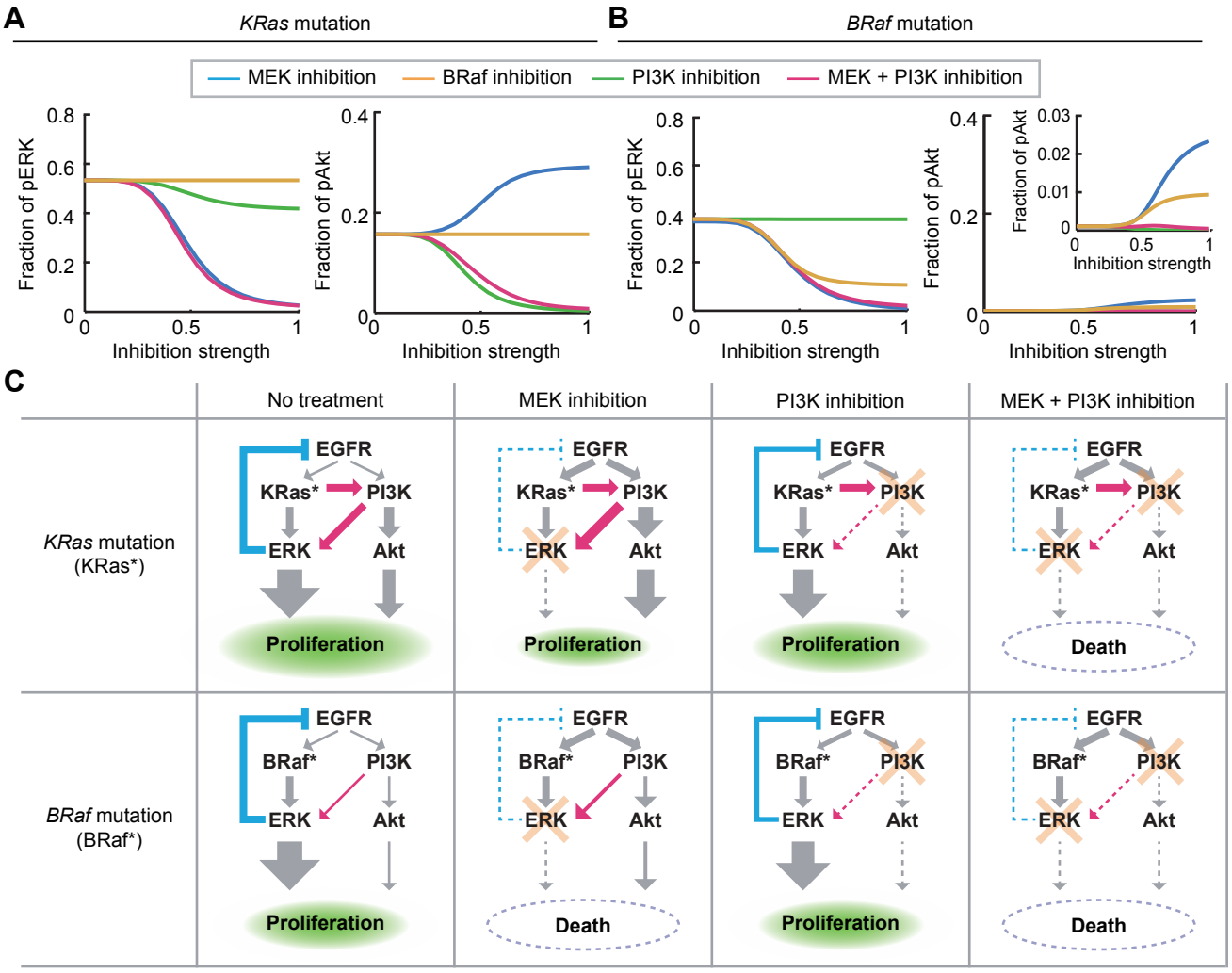
A
KRas mutation
B
BRaf mutation
MEK inhibition
BRaf inhibition
PI3K inhibition
MEK + PI3K inhibition
Fraction of pERK
Fraction of pAkt
Inhibition strength
C
No treatment
MEK inhibition
PI3K inhibition
MEK + PI3K inhibition
KRas mutation (KRas*)
BRaf mutation (BRaf*)
EGFR
KRas*
BRaf*
PI3K
ERK
Akt
Proliferation
Death